Fouda et al. Nanoscale Research Letters (2016) 11:13
DOI 10.1186/s11671-015-1221-8

Nanoscale Research Letters
a SpringerOpen Journal

NANO COMMENTARY Open Access

Photo-Response of Functionalized Self-Assembled Graphene Oxide on Zinc Oxide Heterostructure to UV Illumination

A. N. Fouda[1,2*], A. B. El Basaty[3] and E. A. Eid[4]

Abstract

Convective assembly technique which is a simple and scalable method was used for coating uniform graphene oxide (GO) nanosheets on zinc oxide (ZnO) thin films. Upon UV irradiation, an enhancement in the on-off ratio was observed after functionalizing ZnO films by GO nanosheets. The calculations of on-off ratio, the device responsivity, and the external quantum efficiency were investigated and implied that the GO layer provides a stable pathway for electron transport. Structural investigations of the assembled GO and the heterostructure of GO on ZnO were performed using scanning electron microscopy (SEM), transmission electron microscopy (TEM), X-ray diffraction (XRD), and Fourier transform infrared spectroscopy (FTIR). The covered GO layer has a wide continuous area, with wrinkles and folds at the edges. In addition, the phonon lattice vibrations were investigated by Raman analysis. For GO and the heterostructure, a little change in the ratio between the D-band and G-band was found which means that no additional defects were formed within the heterostructure.

Keywords: Structure modeling, Graphene oxide on ZnO, Self-assembly, Raman analysis

Background

Much attention has been attracted to the coupling of graphene oxide (GO) and graphene (GR) with some semiconductors, which makes a proper enhancement in the charge transport, photocatalytic activity, and thermal conductivity [1–4]. In particular, GO/ZnO heterostructure is desirable for the inverted structure of hybrid solar cells [5], transparent electrode in optoelectronic devices [6], photocatalytic active devices [7], and sensors [8]. Zinc oxide (ZnO) has a large exciton binding energy of 59 meV, wide band gap of 3.37 eV at room temperature, piezoelectricity, catalytic activity, low cost in production, and bio-compatibility and is non-toxic (environmental friendly) and chemically stable [9, 10]. It has a wide range of applications, like transparent electrodes, gas sensors, dilute magnetic semiconductors (DMS), window layer for solar cells, active channel layer of transparent thin film transistor (TTFT), photocatalysts, surface acoustic wave devices, microsensors, and photodetectors [11, 12].

Graphene, a flat monolayer of two-dimensional (2D) honeycomb carbon atoms, has a wide range of applications due to its superior structural and electronic properties [13–15]. It can be synthesized by several methods, including micromechanical exfoliation [16], thermal expansion [17], chemical vapor deposition [18], and reduction from GO [19, 20]. Recently, there has been much progress in the self-assembly of nano-colloidal particles for photonics, sensors, supercapacitors, electronics, and other applications. Self-assembly technique provides a facile, rapid, inexpensive, scalable, controllable, and good way to deposit nano- and micrometer-sized particles. Controlling the interactions among particles and particle kinetics is required for device fabrication using the self-assembly method [21–23]. The colloidal composition, concentration, and system setup were considered while performing the experiment (more details about the experiment procedure can be found in the "Experimental" section).

Some studies have primarily focused on ZnO-based photodetectors [24–27]. ZnO-based nanostructured photodetectors exhibited a relatively long response time

* Correspondence: alynabieh@yahoo.com
[1]Physics Department, Faculty of Science, Suez Canal University, Ismailia 41522, Egypt
[2]Recruitment Department, University of Hail, Hail 2440, Kingdom of Saudi Arabia
Full list of author information is available at the end of the article

[28]. However, building an electric field within a heterostructure junction is one of the strategies to separate and transport the photo-carriers [29]. In the open literatures, there are some attempts to introduce GR-ZnO nano-composites, ZnO nanowires, GR arrays/films [30, 31], GR-ZnO nanorods [32, 33], and GR wrapped to hollow ZnO spheres [34]. Moreover, resistance switching of GR to ZnO as a resistive random access memory was reported [35]. However, the reports on the assembly of GO on ZnO films and the application of GO/ZnO heterostructure in UV sensing are still quite rare. Here, a low-cost, facile, and scalable technique was used to cover ZnO films by GO nanosheets. We used ZnO thin films as a template for GO to improve the separation efficiency of photo-generated electron hole pairs upon UV irradiation. This hybrid heterostructure exhibited a repeated fast and uniform response to UV illumination because of the high-transport properties of carbon nanostructures.

Experimental

A schematic diagram for the experimental work is shown in Fig. 1 which can be summarized in three steps. In the first step, 150-nm-thick ZnO thin films were grown on an *a*-plane sapphire substrate using radio-frequency magnetron sputtering technique at deposition temperature of 600 °C, working pressure of 5×10^{-4} Torr, background pressure of 2×10^{-6} Torr, oxygen fraction of 20 %, and vacuum annealed at 850 °C, as described in references [36, 37]. Smooth *a*-plane sapphire substrates were cleaned using organic solvents, rinsed in DI water, and pre-sputtering of the target was performed to remove contaminations before deposition. In the second step, GO was prepared by chemical oxidation of graphite according to the well-known modified Hummers' method. A full detailed description of the preparation procedure can be found elsewhere [19, 20]. In the third step, convective assembly technique was used to deposit a continuous thin layer (10 nm) of GO on the prepared ZnO thin films. The convective assembly setup is as follows: a cleaned glass substrate was oriented at 45° with respect to a ZnO film and acts as a knife blade. Eighty microliters of a well-dispersed GO meniscus (1 mg/mL) was injected between the blade and the ZnO film. Then, a slow motion of the blade with a step motor at a speed of 1 cm/h was performed.

Structural characterizations were performed using X-ray diffraction (XRD), field emission scanning electron microscopy (FE-SEM), transmission electron microscopy (TEM), and Raman spectroscopy. Burker-D8 diffractometer with Cuk_{α} radiation was used for XRD measurements. The surface morphology was investigated using FE-SEM (Helios 400). The nano-scale structures were monitored using transmission electron microscopy (model JEM 1230, JEOL,

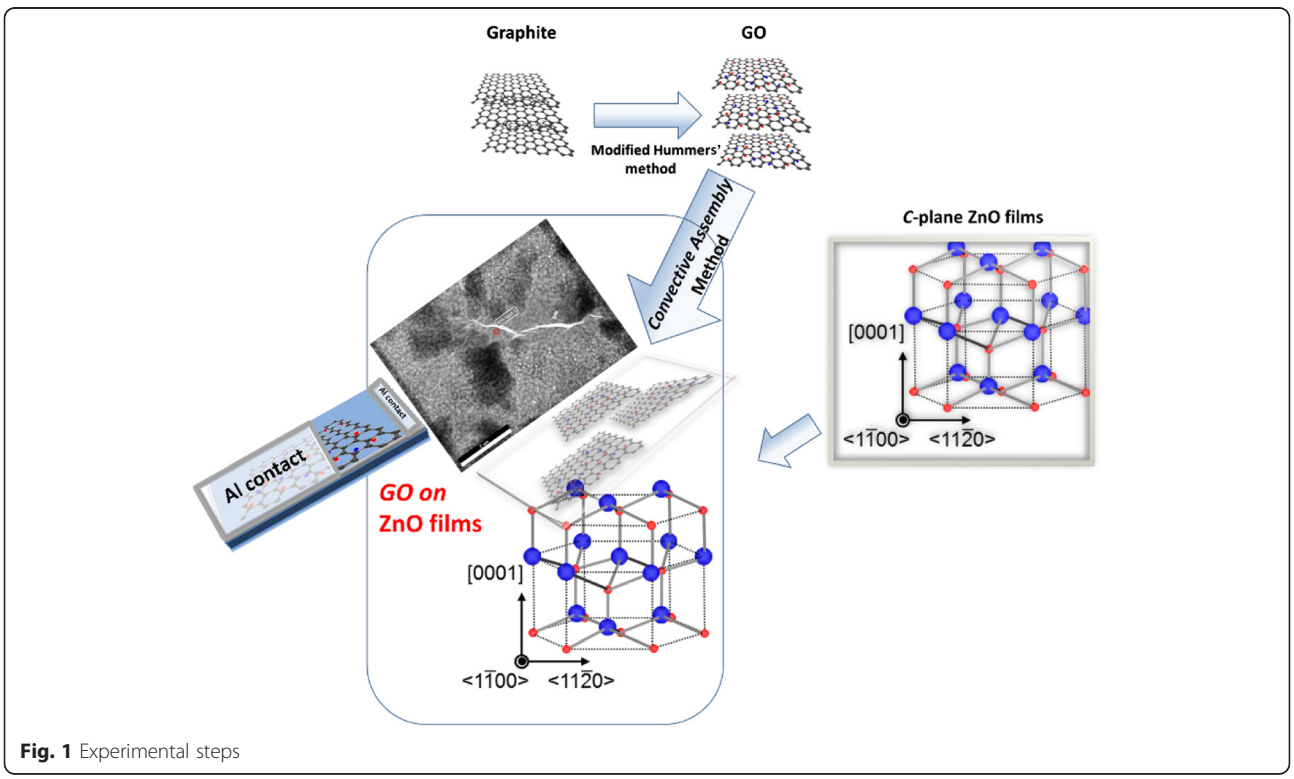

Fig. 1 Experimental steps

Japan). The characterizations were extended to the lattice vibration modes by micro-Raman spectroscopy measurements at room temperature (model Renishaw System 2000) with Ar^+ laser at wavelength of 514 nm and power of 3 mW. To evaluate the photoconductivity of the samples, a patterned mask was used to deposit 20-nm-thick Al electrodes (4 mm wide) by thermal evaporation technique as shown in Fig. 1. I-V characteristics were measured at room temperature by a Keithley electrometer (model 6517B). A UV source (254 nm) with power density of 250 mW cm^{-2} was used to irradiate the samples.

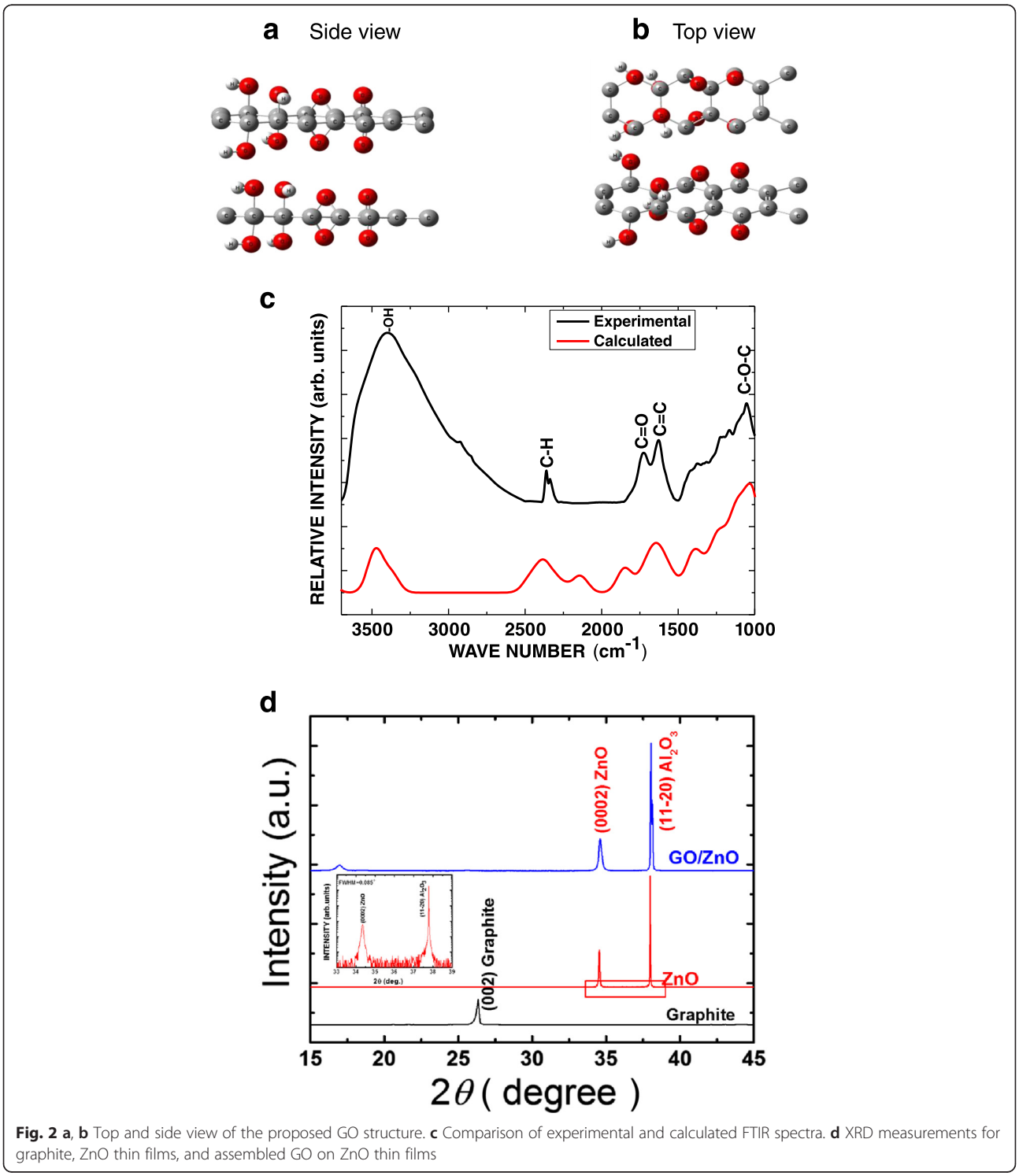

Fig. 2 **a**, **b** Top and side view of the proposed GO structure. **c** Comparison of experimental and calculated FTIR spectra. **d** XRD measurements for graphite, ZnO thin films, and assembled GO on ZnO thin films

Discussion

Direct information about GO structure can be obtained hardly which attracts attention to its structure modeling. Structure is built with Gaussian view program. Structure modeling of GO has been done using Gaussian 03W program. Finally, the output calculations are represented

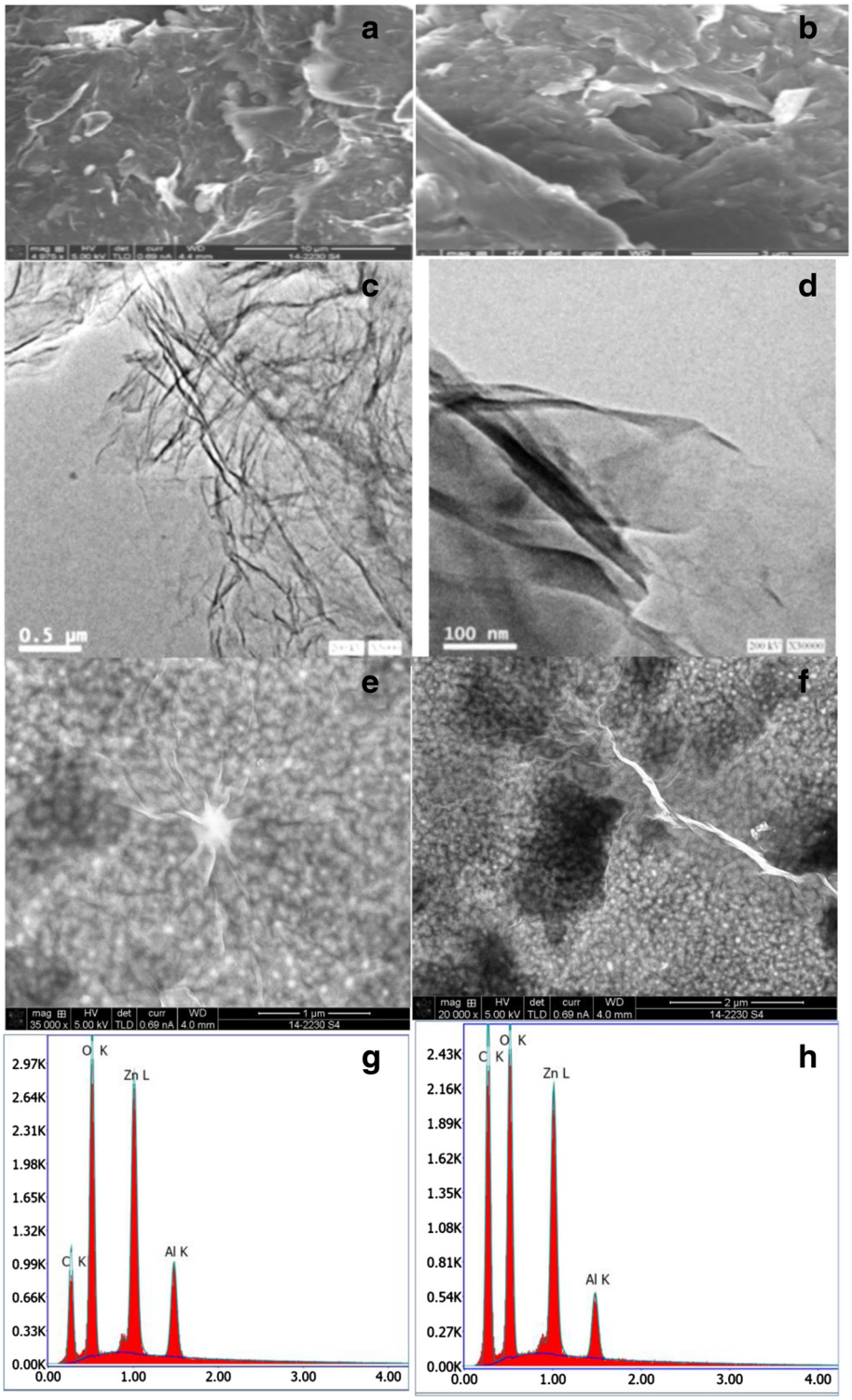

Fig. 3 **a**, **b** SEM images of GO nanosheets. **c**, **d** TEM images of GO nanosheets. **e**, **f** FE-SEM images of deposited GO on ZnO films. **g**, **h** EDAX spectra of deposited GO on ZnO films

by Chemcraft program as IR spectrum. The following rules were considered while proposing a stable GO structure [38–42]. First, GO contains sp^2 and sp^3 orbital hybridization. Second, GO consists of a graphene layer with hydroxyl and carbonyl functional groups. Third, an equal number of the functional groups is built on each side of the graphene sheet. Fourth, each carbon atom cannot be attached with two functional groups. The proposed structure is shown in Fig. 2a (side view) and Fig. 2b (for the top view). Figure 2c shows partial overlap of experimental IR spectrum with the theoretically calculated IR spectrum. The calculations were performed according to the density functional theory (DFT) method using Gaussian 03W program. The peak at 1682.3 cm^{-1} was assigned to the un-oxidized graphitic domains (C = C), and an obvious peak at 3399.0 cm^{-1} was attributed to OH stretching vibrations of the adsorbed water molecules. In addition, the peak at 1725.1 cm^{-1} was assigned to the C = O stretching vibration from the carboxyl and carbonyl groups [19, 39]. Hence, during the oxidation, the original extended conjugated π-orbital of graphite was eliminated and replaced by the oxygen-containing functional groups which settled in the carbon skeleton. This result indicates that the proposed GO structure is close to the synthesized GO structure.

Representative XRD patterns of graphite, ZnO films, and GO on ZnO films are shown in Fig. 2d. For ZnO films on an *a*-plane sapphire substrate, a well-oriented (0002) ZnO peak can be observed beside the reflexes of the substrate. In the inset of Fig. 2d, the symmetric nature, sharpness of the (0002) peak with full width at half maximum (FWHM) of 0.087°, and the absence of reflections from other planes confirm a good *c*-axis orientation perpendicular to the (11–20) plane of the sapphire substrate. The distinct sharp (002) peak of graphite was observed at 2θ of 26.55°. After exfoliation, the (002) peak is shifted to a lower angle for GO nanosheets on ZnO films which is related to the increase in the inter-planar spacing beside the reflections of ZnO films and the substrate.

The surface morphology of GO nanosheets is depicted in Fig. 3a, b. It was found that GO flakes have wrinkles and folds at the edges. Moreover, the shown TEM images in Fig. 3c, d clarify that the synthesized GO nanosheets have few layers with a dimension of few hundred nanometers. The ultra-smooth [36, 37] and well-oriented ZnO thin films with root mean square roughness of 0.3 nm act as a template for the assembled GO nanosheets. On the other hand, after the deposition of GO layer on the template, a detectable continuous, wide area and slightly stacked GO nanosheets were observed (see Fig. 3e, f). The chemical composition of the assembled GO/ZnO/Al_2O_3 has been elucidated using EDAX. Only elements of C, Zn, O, and Al can be observed in Fig. 3g, h, which confirm the purity and quality of the prepared samples.

Micro-Raman measurements have been carried out to investigate the quality of the prepared samples. Figure 4 represents the room temperature Raman spectrum of ZnO films, GO nanosheets, and GO on ZnO films. It is very clear from the figure that the Raman spectrum of

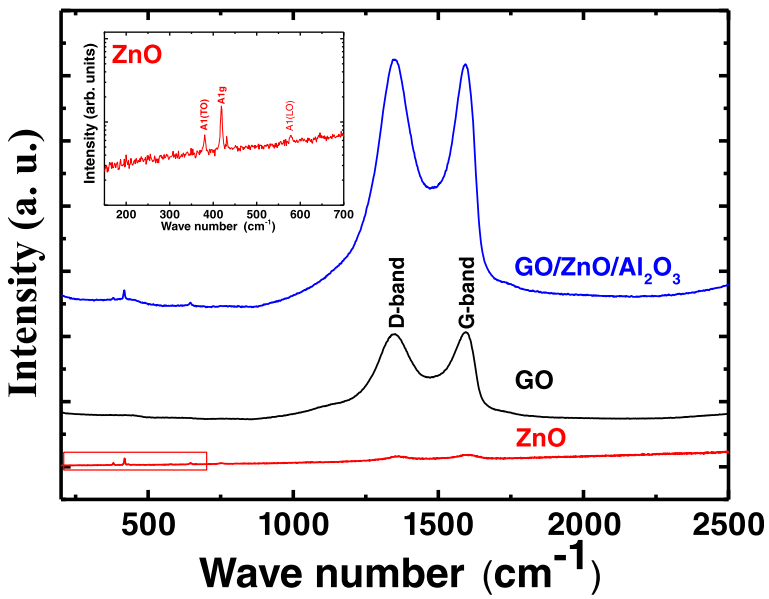

Fig. 4 Raman spectrum of ZnO thin films, GO nanosheets, and GO on ZnO thin films. *Inset* magnifies the shown range for ZnO films

GO exhibited two peaks at 1595 cm^{-1} and 1352 cm^{-1}, respectively. Conventionally, the peak at 1352 cm^{-1} is attributed to the defects, and disorders arise in the sp^2 carbon rings (D-band). The other peak around 1595 cm^{-1} is due to the scattering of the first-order phonons (E_{2g}) which are usually called G-bands [43, 44]. The inset of Fig. 4 magnifies the shown range of Raman spectra for ZnO films. One can see that ZnO transverse optical mode A1(TO) and longitudinal optical mode A1(LO) appeared at 380 and 576 cm^{-1}, respectively [45, 46]. The other peak is at 417, and 650 is attributed to the Al_2O_3 substrate [47, 48]. After the assembly of GO on ZnO, in addition to the G- and D-bands of GO, the characteristic ZnO and sapphire modes can be observed. However, the intensity ratio between the G-band and the D-band (I_G/I_D) has been changed from 1.01 for GO alone to 0.99 after the assembly of GO on ZnO films. The small change in the ratio implies that there is no additional defect introduced in the case of GO/ZnO [49].

We exposed ZnO and GO/ZnO heterostructures to UV illumination, and the output currents were recorded using the Keithley electrometer as a function of applied

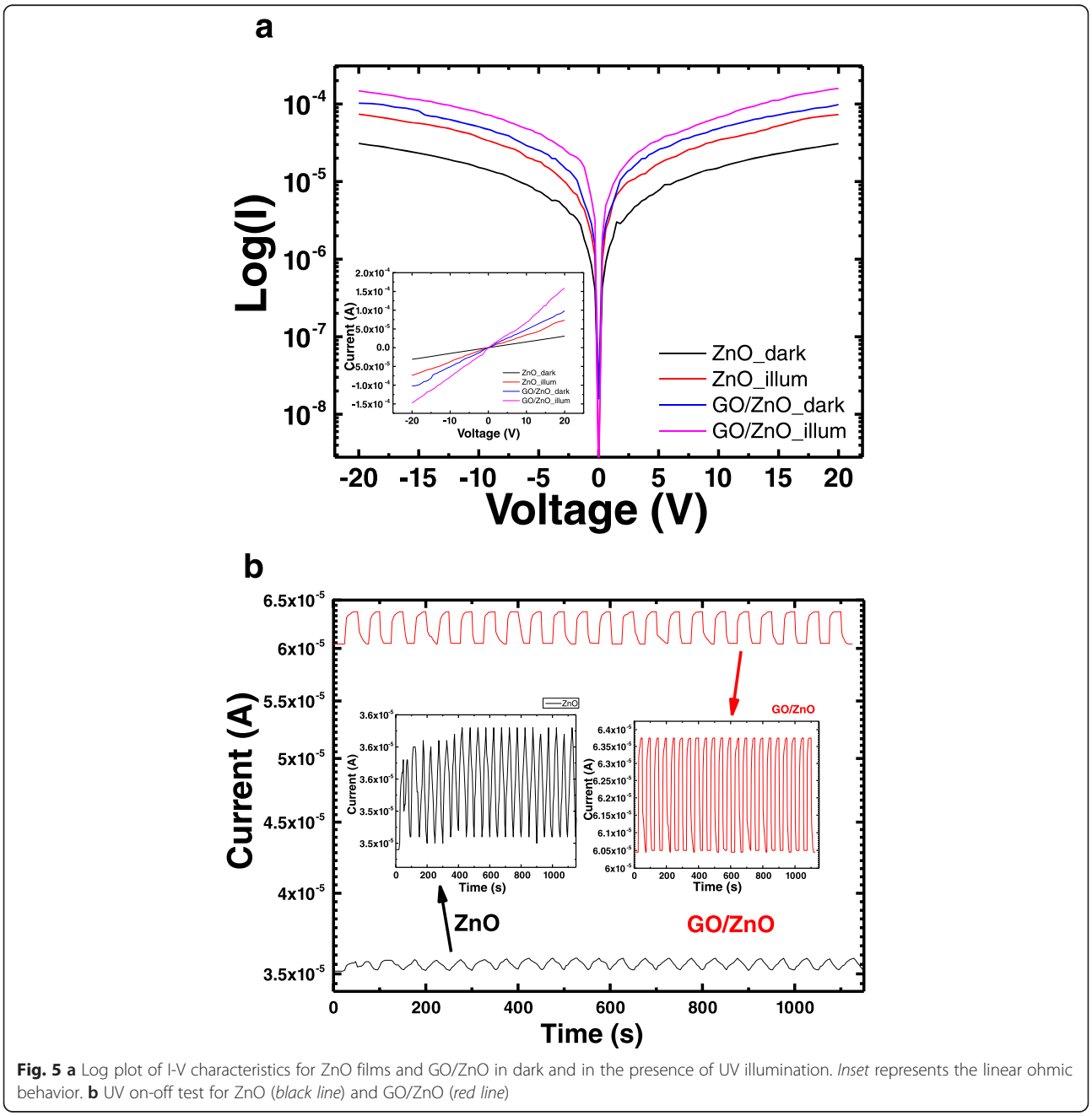

Fig. 5 **a** Log plot of I-V characteristics for ZnO films and GO/ZnO in dark and in the presence of UV illumination. *Inset* represents the linear ohmic behavior. **b** UV on-off test for ZnO (*black line*) and GO/ZnO (*red line*)

voltage. All the samples follow ohmic behavior and the current increase with increasing the applied bias as shown in a linear plot (inset of Fig. 5a) and an algorithmic plot (Fig. 5a). Under UV illumination, a dramatic increase of current was recorded. The generated photocurrent of GO/ZnO was compared with that of ZnO films. Upon irradiation of the heterostructure, the increase in current can be explained in terms of photogenerated electrons which were collected and transported through the paths provided by GO nanosheets since carbon nanostructures have high electron acceptor ability and improve the electron transport properties [50]. Therefore, electrons move from the valance band to the conduction band of ZnO, finding a transport path through GO nanosheets [51]. In order to confirm the feasibility of the prepared heterostructure for UV sensing applications, an on-off test was measured. The applied bias during on/off was 10 V. With alternating switch on and switch off events, a fast and stable photocurrent was detected in the case of the heterostructure (Fig. 5b). In comparison, there was no similar response of ZnO films. Electron hole pairs are generated when the UV illumination is on, and the generated carriers are easily transported through the heterostructure. On the other hand, electron hole pairs recombine quickly when UV illumination is turned off. The recovery speed of the heterostructure is much faster than ZnO films, and the generated photocurrent by GO/ZnO heterostructure was about two times as high as that of ZnO films. Moreover, response current (I_{ph}) was used to calculate the on-off ratio of photocurrent where $I_{ph} = I_{UV} - I_d$, where I_d is the current in dark and I_{UV} is the current under UV illumination condition [33]. The on-off ratio of photocurrent is defined as I_{ph}/I_d. The photocurrent on-off ratio of heterostructure and ZnO films were 0.055 and 0.016, respectively. It is well known that UV sensing of ZnO is related to the absorption and desorption of oxygen molecules on ZnO surface and GO nanosheets enhance the carrier transport [30]. Additionally, the device responsivity R_s can be calculated from the following equation: $R_s = (I_{ph}/P_o A)$, where P_o is the UV power density, A the active area, and I_{ph} the response current. The calculations were extended to the external quantum efficiency of the photodetector which can be calculated by $\mathrm{EQE} = \frac{R_s \times h\vartheta}{e} \times 100$, where hv is the energy of the incident photon [52]. R_s and EQE for ZnO heterostructure were 37×10^{-4} A/W and 1.8 %, respectively, while their values were only 6.2×10^{-4} A/W and 0.3 % for ZnO films. Therefore, the UV photo-response performance of GO/ZnO heterostructure is much higher than ZnO films. The obtained R_s value is consistent with the data reported for graphene sheet-based photodetectors (0.1 ~ 0.5 mA/W) [53].

Conclusion

Surface functionalization of ZnO films by the GO layer was conducted by self-assembly technique. ZnO films act as a good template for the deposited GO layer because of its smoothness. It is worth noting that we emphasized the enhancement in the UV photo-response performance for GO/ZnO heterostructure with respect to ZnO films. Since GO creates two-dimensional electronic-conducting channels for the photo-generated carriers, separation and transport of photo-generated electron hole pairs and reducing the recombination improve the on-off ratio.

Competing interests

The authors declare that they have no competing interests.

Authors' contributions

ANF proposed the point on the assembly of the GO layer on the ZnO template, shared in the setup of the UV experiment, helped in the analysis of the experimental results, and co-wrote the paper. EAE designed the template and conducted XRD and FE-SEM analyses. ABEB carried out the UV photo-response experiment and co-wrote the manuscript. All authors read and approve the current manuscript.

Author details

[1]Physics Department, Faculty of Science, Suez Canal University, Ismailia 41522, Egypt. [2]Recruitment Department, University of Hail, Hail 2440, Kingdom of Saudi Arabia. [3]Basic Science Department, Faculty of Industrial Education, Helwan University, Cairo, Egypt. [4]Department of Basic Science, Higher Technological Institute, 10th of Ramadan City, Egypt.

Received: 15 October 2015 Accepted: 27 December 2015
Published online: 12 January 2016

References

1. Liu W, Cai J, Li Z (2015) Self-assembly of semiconductor nanoparticles/reduced graphene oxide (RGO) composite aerogels for enhanced photocatalytic performance and facile recycling in aqueous photocatalysis. ACS Sustainable Chem Eng 3(2):277–5
2. Gao N, Fang X (2015) Synthesis and development of graphene-inorganic semiconductor nanocomposites. Chem Rev 115(16):8294–46
3. Yang M-Q, Zhang N, Pagliaro M, Xu Y-J (2014) Artificial photosynthesis over graphene-semiconductor composites. Are we getting better? Chem Soc Rev 43:8240–14
4. Xing M, Shen F, Qiu B, Zhang J (2014) Highly dispersed boron doped graphene nanosheets loaded with TiO_2 nanoparticles for enhancing CO_2 photoreduction. Sci Rep 4:6341–7
5. Park H, Chang S, Jean J, Jayce J, Cheng J, Araujo PT et al (2013) Graphene cathode-based ZnO nanowire hybrid solar cells. Nano Lett 13:233–6
6. K Hasan, MO. Sandberg, O Nur, M Willander. Transparent electrodes: ZnO/polyfluorene hybrid LED on an efficient hole-transport layer of graphene oxide and transparent graphene electrode. Adv. Opt. Mater. 2014; 2(4): 304: doi:10.1002/adom.201470021.
7. Pan X, Yang MQ, Xu Y-J (2014) Morphology control defect engineering and photoactivity tuning of ZnO crystals by graphene oxide-a unique 2D macromolecular surfactant. Phys Chem Chem Phys 16:5589–10
8. Biroju RK, Tilak N, Rajender G, Dhara S, Giri PK (2015) Catalyst free growth of ZnO nanowires on graphene and graphene oxide and its enhanced photoluminescence and photoresponse. Nanotechnol 26:145601–12
9. Look DC, Hemsky JW, Sizelove JR (1999) Residual native shallow donor in ZnO. Phys Rev Lett 82:2552
10. Jagadish C, Pearton S (2006) Zinc oxide bulk, thin films and nanostructures. Elsevier Ltd., Oxford, Ox5 1GB, UK
11. Shinde SS, Rajpure KY (2012) Fabrication and performance of N-doped ZnO UV photoconductive detector. J Alloys Compd 522:118–4
12. Gonzalez Vallsa I, Lira Cantu M (2009) Vertically-aligned nanostructures of ZnO for excitonic solar cells: a review. Energy Environ Sci 2:19–34

13. Morozov SV, Novoselov KS, Geim AK (2008) Giant intrinsic carrier mobilities in graphene and its bilayer. Phys Rev Lett 100:16602–2
14. Castro Neto AH, Guinea F, Peres NMR, Novoselov KS, GeimAK (2009) The electronic properties of graphene. Rev Mod Phys 81:109–55
15. Rani A, Nam SW, Park M (2010) Electrical conductivity of chemically reduced graphene powders under compression. Carbon Lett 11(2):90–5
16. Schniepp H, Li J, Aksay I (2006) Functionalized single graphene sheets derived from splitting graphite oxide. J Phys Chem B(110):8535–4
17. Novoselov K, Geim A, Morozov SV, Jiang D, Zhang Y, Dubonos SV, Grigorieva IV, Firsov AA (2004) Electric field effect in atomically thin carbon films. Science 306:666–3
18. Duraia E-SM, Mansurov Z, Tokmoldin S (2011) Formation of graphene by the thermal annealing of a graphite layer on silicon substrate in vacuum. Vac 86:232–2
19. Fouda AN, Abu Assy M, El Enany G, Yousf N (2014) Enhanced capacitance of thermally reduced hexagonal graphene oxide for high performance supercapacitor. Fullerenes Nanotubes Carbon Nanostruct 23:618–4
20. Fouda AN, Abu-Assy MK, Yousf N (2014) Structural and capacitive characterizations of high temperature nitrogen annealed graphene oxide. IOSR J Appl Phys 6(2):33–4
21. Liberman V, Yilmaz C, Bloomstein TM, Somu S, Echegoyen Y, Busnaina A et al (2010) A nanoparticle convective directed assembly process for the fabrication of periodic surface enhanced Raman spectroscopy substrates. Adv Mater 22:4298–4
22. Velev OD, Gupta S (2009) Materials fabricated by micro- and nanoparticle assembly-the challenging path from science to engineering. Adv Mater 21:1897–9
23. Prevo BG, Kuncicky DM, Velev OD (2007) Engineered deposition of coatings from nano- and micro-particles: a brief review of convective assembly at high volume fraction. Colloids Surf A Physicochem Eng Asp 311:2–8
24. Wang ZL, Song JH (2006) Piezoelectric nanogenerators based on zinc oxide nanowire arrays. Science 312:242–4
25. Inamdar SI, Rajpure KY (2014) High-performance metal-semiconductor-metal UV photodetector based on spray deposited ZnO thin films. J Alloys Compd 595:55–4
26. Young S-J, Liu Y-H, Hsiao C-H, Chang S-J, Wang B-C, Kao T-H, Tsai K-S, San-Lein W (2014) ZnO-based ultraviolet photodetectors with novel nanosheet structures. IEEE Trans Nanotechnol 13(2):238–7
27. Li QH, Gao T, Wang YG, Wang TH (2005) Adsorption and desorption of oxygen probed from ZnO nanowire films by photocurrent measurements. Appl Phys Lett 86(12):123117
28. Park C, Lee J, Sob H-M, Chang WS (2015) An ultrafast response grating structural ZnO photodetector with back-to-back Schottky barriers produced by hydrothermal growth. J Mater Chem C 3:2737–6
29. Qiao H, Yuan J, Xu Z, Chen C, Lin S, Wang Y et al (2015) Broadband photodetectors based on graphene–Bi_2Te_3 heterostructure. ACS Nano 9(2):1886–8
30. Liu H, Sun Q, Xing J, Zheng Z, Zhang Z, Lu Z, Zhao K (2015) Fast and enhanced broadband photoresponse of a ZnO nanowire array/reduced graphene oxide film hybrid photodetector from the visible to the near-infrared range. ACS Appl Mater Interfaces 7(12):6645–6
31. Chang H, Sun Z, Ho KY-F, Tao X, Yan F, Kwok W-M, Zheng Z (2011) A highly sensitive ultraviolet sensor based on a facile *in situ* solution-grown ZnO nanorod/graphene heterostructure. Nanoscale 3:258–6
32. Boruah BD, Ferry DB, Mukherjee A, Misra A (2015) Few-layer graphene/ZnO nanowires based high performance UV photodetector. Nanotechnol 26:235703–7
33. Fu X-W, Liao Z-M, Zhou Y-B, Wu H-C, Bie Y-Q, Xu J, Yu D-P (2012) Graphene/ZnO nanowire/graphene vertical structure based fast-response ultraviolet photodetector. Appl Phys Lett 100:223114–4
34. Khoa NT, Kim SW, Yoo D-H, Cho S, Kim EJ, Hahn SH (2015) Fabrication of Au/graphene-wrapped ZnO-nanoparticle-assembled hollow spheres with effective photo-induced charge transfer for photocatalysis. ACS Appl Mater Interf 7(6):3524–8
35. Lin C-L, Chang W-Y, Huang Y-L, Juan P-C, Wang T-W, Hung K-Y et al (2015) Resistance switching behavior of ZnO resistive random access memory with a reduced graphene oxide capping layer. Jap J Appl Phys 54:04DJ–08
36. Fouda AN, Duraia E-SM, Eid EA (2014) Ultra-smooth and lattice relaxed ZnO thin films. Superlattice Microstruct 73:268–6
37. Eid EA, Fouda AN (2015) Influence of homo buffer layer thickness on the quality of ZnO epilayers. Spectrochim Acta Part A 149:127–5
38. Rasuli R, Iraji zad A (2010) Density functional theory prediction for oxidation and exfoliation of graphite to grapheme. Appl Surf Sci 256:7596–3
39. Liu L, Lu W, Gao J, Chen Z (2012) Amorphous structural models for graphene oxides. Carbon 50:1690–8
40. Wang L, Lee K, Sun YY, Lucking M, Chen Z, Zhao J, Zhang S (2009) Graphene oxide as an ideal substrate for hydrogen storage. ACS Nano 3:2995–5
41. Yan JA, Xian LD, Chou MY (2009) Structural and electronic properties of oxidized graphene. Phys Rev Lett 103(8):086802
42. Tamura R (2010) Conductance of telescoped double-walled nanotubes from perturbation calculations. Phys Rev B 82:035415
43. Beall G, Duraia E-SM, Yu Q, Liu Z (2014) Single crystalline graphene synthesized by thermal annealing of humic acid over copper foils. Physica E 56:331–5
44. Duraia E-SM, Beall G (2015) Humidity sensing properties of reduced humic acid. Sens Actuators B 220:22–4
45. Ming-Lung T, Sua Y-K, Ma CY (2006) Nitrogen-doped p-type ZnO films prepared from nitrogen gas radio-frequency magnetron sputtering. J Appl Phys 100:053705–4
46. Yahia SB, Znaidi L, Kanaev A, Petitet JP (2008) Raman study of oriented ZnO thin films deposited by sol-gel method. Spectrochim Acta Part A 71:1234–4
47. Wermelinger T, Borgia C, Solenthaler C, Spolenak R (2007) D-Raman spectroscopy measurements of the symmetry of residual stress fields in plastically deformed sapphire crystals. Acta Mater 55:4657–8
48. Jia W, Yen WM (1989) Raman scattering from sapphire fibers. J Raman Spectros 20:785–3
49. Shen J, Hu Y, Li C, Qin C, Shi M, Ye M (2009) Layer-by-layer self-assembly of graphene nanoplatelets. Langmuir 25:6122–6
50. Yin S, Men X, Sun H, She P, Zhang W, Wu C et al (2015) Enhanced photocurrent generation of bio-inspired graphene/ZnO composite films. J Mater Chem A 3:12016–6
51. Wang Z, Zhan X, Wang Y, Muhammad S, Huangb Y, He J (2012) A flexible UV nanosensor based on reduced graphene oxide decorated ZnO nanostructures. Nanoscale 4:2678–6
52. Boruah BD, Mukherjee A, Sridhar S, Misra A (2015) Highly dense ZnO nanowires grown on graphene foam for ultraviolet photodetection. ACS Appl Mater Interf 7(19):10606–6
53. Xia FN, Mueller T, Lin YM, Valdes-Garcia A, Avouris P (2009) Ultrafast graphene photodetector. Nat Nanotechnol 4:839–4